Amini et al., http://www.jcb.org/cgi/content/full/jcb.201310117/DC1

Figure S1. **ANI-1 and NMY-2 localize to the rachis of wild-type hermaphrodites and report on rachis bridge organization.** (A and D) Mid-section confocal images of the germline of wild-type early L3 (top), L4 (middle), and adult (bottom) hermaphrodites coexpressing a membrane marker and GFP::ANI-1 (A) or NMY-2::GFP (D). In all frames, anterior is to the left. Bars, 10 µm. (B and E) Proportion of germ cells showing rachis bridges with a diameter >0.8 µm (turquoise) or <0.8 µm (red) throughout development, as measured by GFP::ANI-1 (B) and NMY-2::GFP (E) fluorescence distribution. (C and F) Maximal rachis bridge diameter in germ cells of animals in various developmental stages, as measured with fluorescence distribution of the membrane marker (red) and GFP::ANI-1 (C, green) or NMY-2::GFP (F, green). Error bars represent SD. In B, C, E, and F, the numbers in brackets represent the total number of germ cells analyzed. The results on rachis bridge organization obtained with these markers are identical to those obtained after analysis of GFP::ANI-2 (Fig. 3).

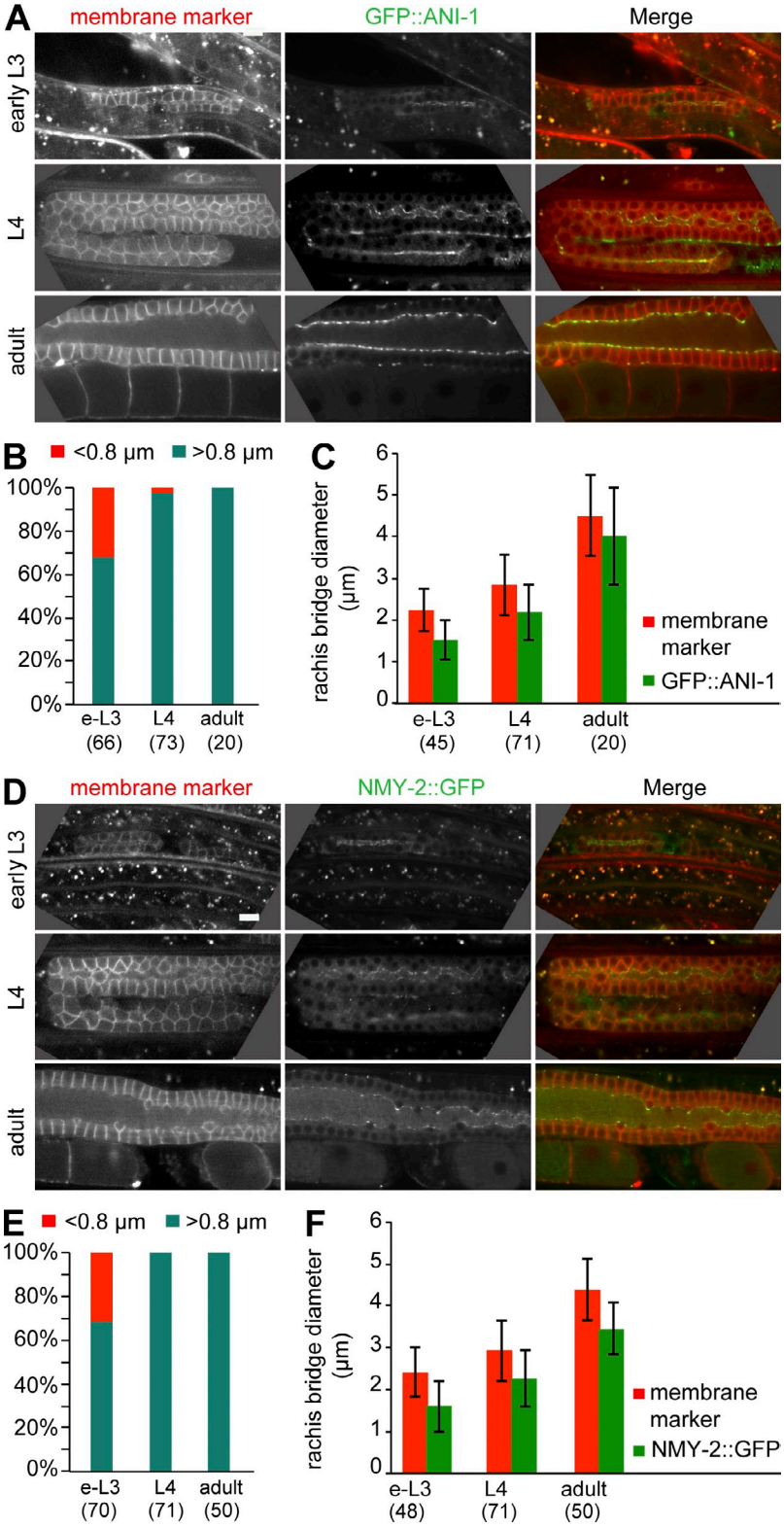

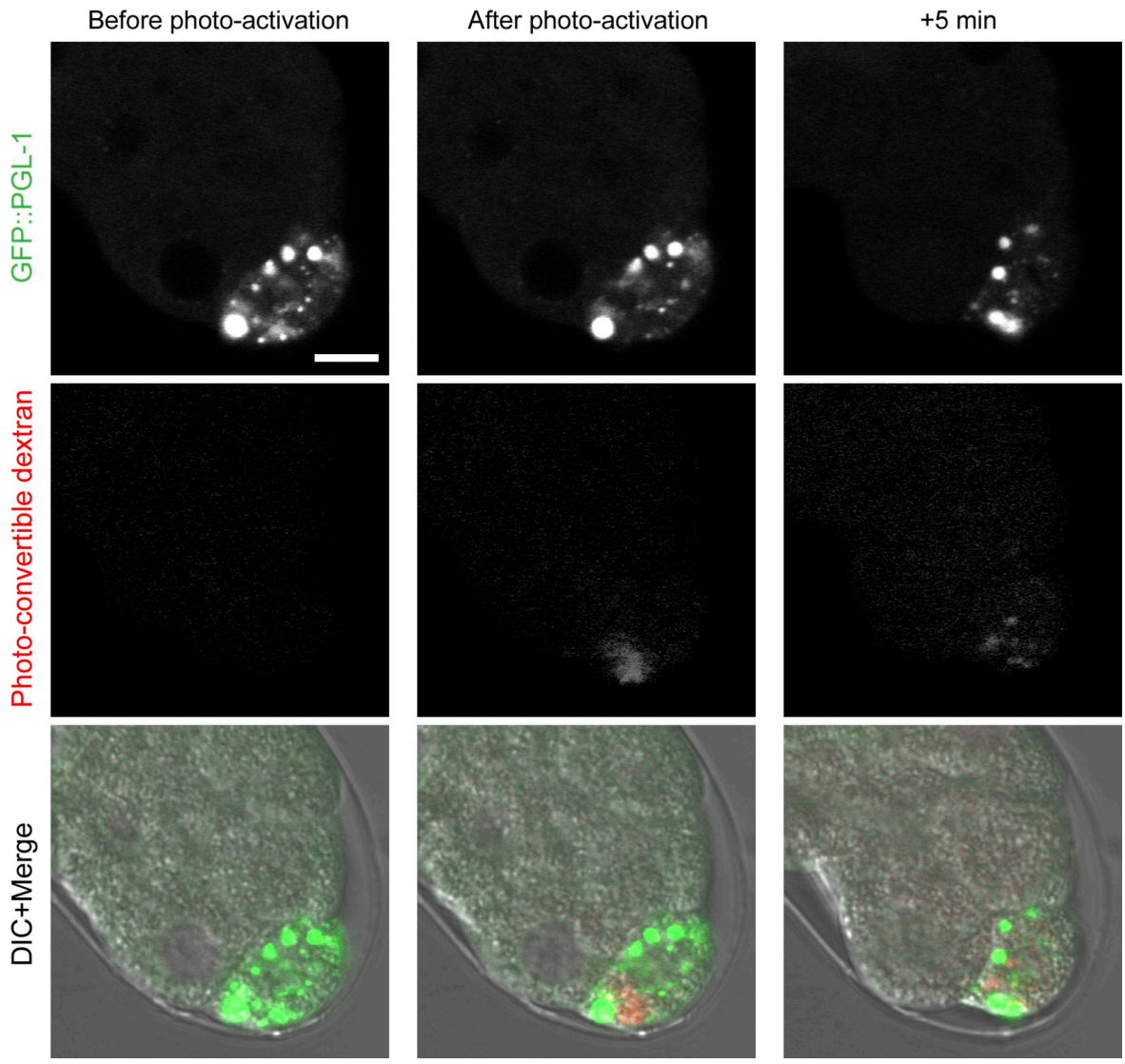

Figure S2. **Molecule diffusion in the cytoplasm of embryonic blastomeres.** Mid-section confocal images of an embryo expressing GFP::PGL-1 exogenously supplied with photo-convertible rhodamine-dextran. After photoactivation in part of the P_3 blastomere, the fluorescent signal rapidly spread throughout the cell. Bar, 10 μm.

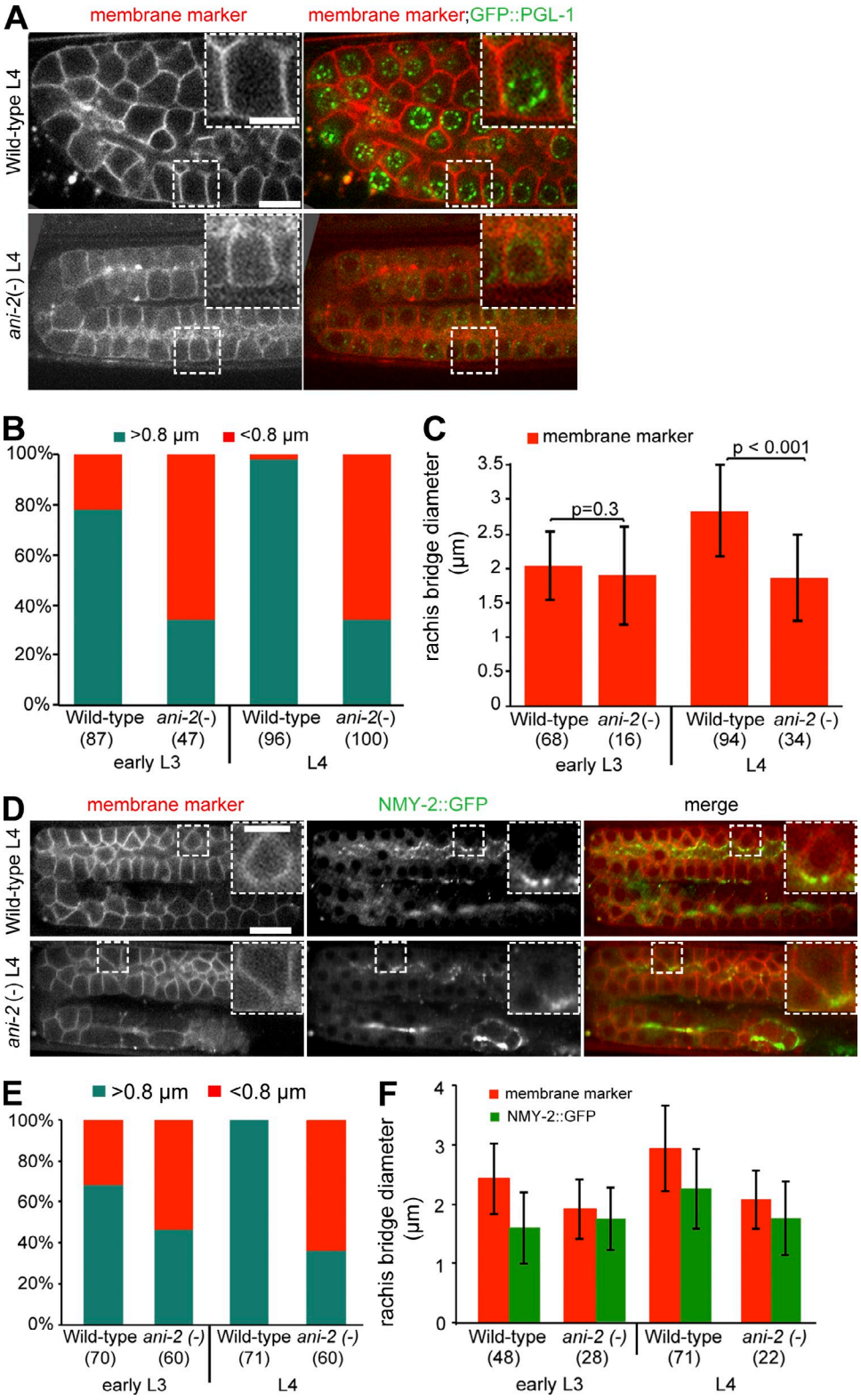

Figure S3. **ANI-2 is required for rachis bridge stability.** (A and D) Mid-section confocal images of the germline of a wild-type and an *ani-2*(−) L4 hermaphrodite expressing a membrane marker (red) and GFP::PGL-1 (A, green) or NMY-2::GFP (D, green). Bar, 10 µm. The regions delineated by the white dashed square are magnified in the inset (bar for insets, 5 µm). (B and E) Proportion of germ cells showing rachis bridges with a diameter >0.8 µm (turquoise) or <0.8 µm (red) in wild-type and *ani-2*(−) animals at the L3 and L4 larval stages, as measured by distribution of the membrane marker alone (B) or together with NMY-2::GFP (E). (C and F) Maximal rachis bridge diameter in germ cells of wild-type and *ani-2*(−) animals at the L3 and L4 larval stages, as measured with distribution of the membrane marker alone (red) or together with NMY-2::GFP (green). Rachis bridges that are <0.8 µm in diameter are excluded from this analysis. Error bars represent SD. In B, C, E, and F the numbers in brackets represent the total number of germ cells analyzed. The results on rachis bridge organization obtained with these markers are identical to those obtained after analysis of GFP::ANI-1 (Fig. 4).

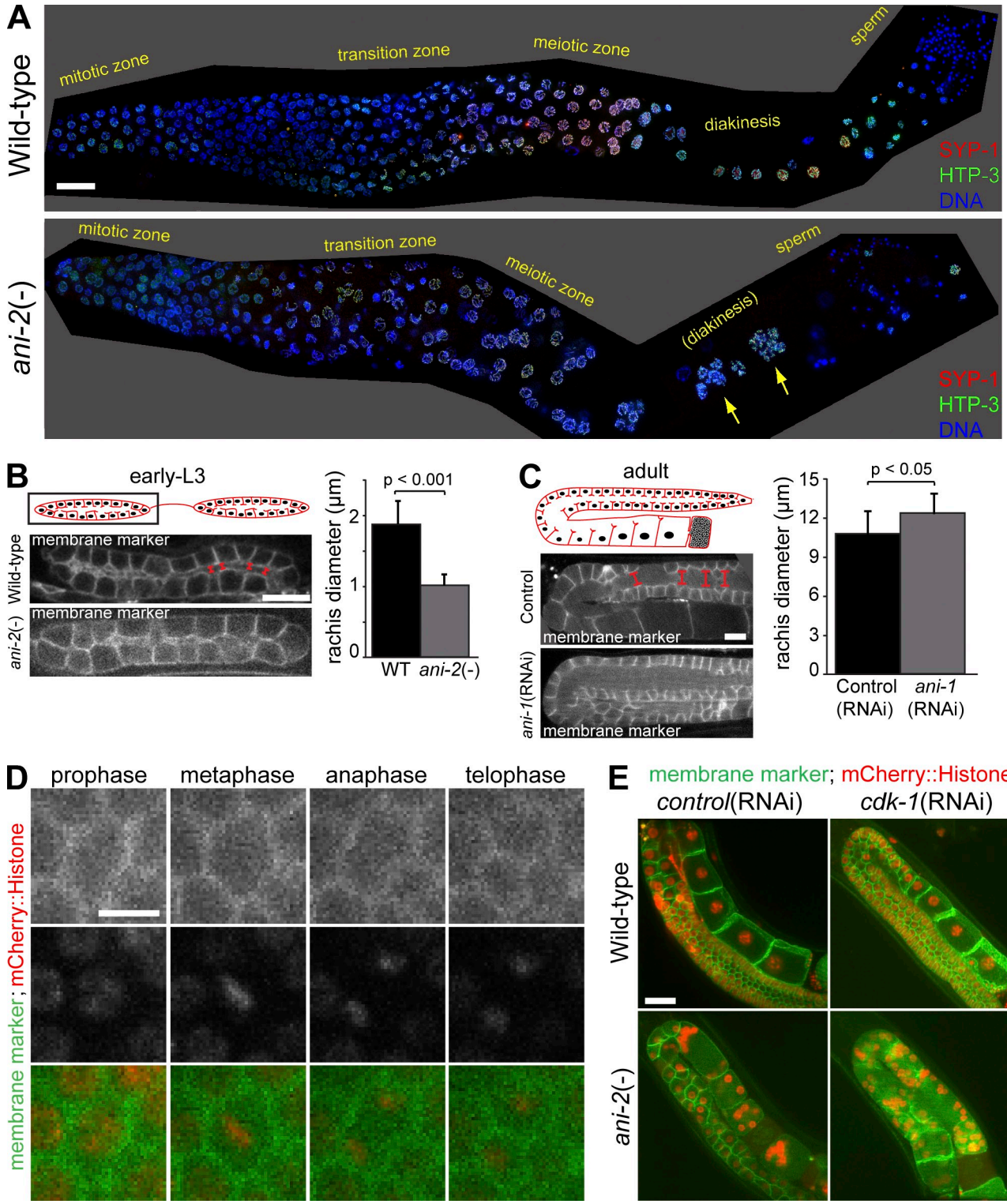

Figure S4. **Phenotypic analysis of *ani-2* mutants.** (A) Projected image stacks of fixed extruded gonads from wild-type (left) and *ani-2*(−) young adult hermaphrodites immunostained with SYP-1 (red), HTP-3 (green), and DAPI (blue). Arrows point to germ cells with defect in diakinesis. Each image was assembled from multiple acquisitions of the same gonad. Bar, 20 µm. (B) Schematic representation of the gonad and images of one gonad in wild-type and *ani-2*(−) mutant early L3 stage larvae. Rachis diameter was measured in multiple regions and confocal sections of the gonad (red line). The graph represents the average diameter of the rachis in wild-type and *ani-2*(−) mutant L3 stage larvae. Rachis diameter is significantly reduced in *ani-2*(−) mutants compared with the wild type. (C) Schematic representation of the gonad and images of one gonad in control and *ani-1(RNAi)* adult animals. Figure elements are as in B. Rachis diameter is significantly increased in *ani-1(RNAi)* animals compared with control. (D) Time-lapse confocal images of a germline stem cell dividing in the gonad of an *ani-2*(−) hermaphrodite. The cell properly progresses through all stages of M phase. Bar, 5 µm. (E) Mid-section confocal images of the germline of wild-type and *ani-2*(−) adult hermaphrodites expressing a membrane marker (green) and mCherry::Histone H2B (red). Blocking cell cycle progression with *cdk-1(RNAi)* (right) did not preclude germ cell multinucleation, indicating that it is not a consequence of inappropriate reentry into the cell cycle. Bar, 10 µm.

Video 1. **Analysis of gonad elastic deformation during ovulation in a wild-type hermaphrodite.** Time-lapse movie of the gonad of a wild-type hermaphrodite expressing GFP::ANI-2 (green) and a membrane marker (red) captured during ovulation. Images were captured every 30 s with a swept field confocal microscope (Nikon), and maximal-intensity projections are played at 10 images/s.

Video 2. **Analysis of gonad elastic deformation during ovulation in a hermaphrodite partially depleted of ANI-2.** Time-lapse movie of the gonad of a hermaphrodite partially depleted of ANI-2 and expressing GFP::ANI-2 (green) and a membrane marker (red) captured during ovulation. Images were captured every 30 s with a swept field confocal microscope (Nikon), and maximal-intensity projections are played at 10 images/s.

Table S1. ***C. elegans* strains used in this study**

Strain no.	Genotype
N2	Wild-type Bristol strain
VC703	*ani-2(ok1147)/mIn1[mIs14 dpy-10(e128)] II*
OD95	*unc-119(ed3) III; ltIs37 [Ppie-1::mCherry::his-58; unc-119(+)] IV; ltIs38 [Ppie-1::gfp::PH(PLC1delta1); unc-119(+)]*
UM185	*unc-119(ed3) III; ltIs44 [Ppie-1::mCherry::PH(PLC1delta1); unc-119(+)] IV; axIs1720 [Ppie-1::gfp::pgl-1::pgl-1 3′; unc-119(+)]*
UM186	*ani-2(ok1147)/mIn1[mIs14 dpy-10(e128)] II; ltIs44 [Ppie-1::mCherry::PH(PLC1delta1); unc-119(+)] IV; axIs1720 [Ppie-1::gfp::pgl-1::pgl-1 3′; unc-119(+)]*
UM208	*unc-119(ed3) III; ltIs81 [Ppie-1::gfp-TEV-Stag::ani-2; unc-119 (+)]; ltIs44 [Ppie-1::mCherry::PH(PLC1delta1); unc-119(+)] IV*
OD182	*unc-119(ed3) III; ltIs28 [Ppie-1::gfp-TEV-Stag::ani-1; unc-119 (+)]; ltIs44 [Ppie-1::mCherry::PH(PLC1delta1); unc-119(+)] IV*
UM341	*ani-2(ok1147)/mIn1[mIs14 dpy-10(e128)] II; unc-119(ed3) III; ltIs28 [Ppie-1::gfp-TEV-Stag::ani-1; unc-119 (+)]; ltIs44 [Ppie-1::mCherry::PH(PLC1delta1); unc-119(+)] IV*
OD183	*unc-119(ed3) III; ltIs44 [Ppie-1::mCherry::PH(PLC1delta1); unc-119(+)] IV; zuIs45 [Pnmy-2::nmy-2::gfp; unc-119 (+)] V*
UM342	*ani-2(ok1147)/mIn1[mIs14 dpy-10(e128)] II; unc-119(ed3) III; ltIs44 [Ppie-1::mCherry::PH(PLC1delta1); unc-119(+)] IV; zuIs45 [Pnmy-2::nmy-2::gfp; unc-119 (+)] V*
JH2107	*unc-119(ed3) III; axIs1720 [Ppie-1::gfp::pgl-1::pgl-1 3′; unc-119(+)]*
UM209	*ani-2(ok1147)/mIn1[mIs14 dpy-10(e128)] II; ltIs37 [Ppie-1::mCherry::his-58; unc-119(+)] IV; ltIs38 [Ppie-1::gfp::PH(PLC1delta1); unc-119(+)]*
JK2879	*gld-2(q497) gld-1(q485) I/hT2[qIs48] (I;III)*
UM230	*gld-2(q497) gld-1(q485) I/hT2[qIs48] (I;III); ani-2(ok1147)/mIn1[mIs14 dpy-10(e128)] II; ltIs37 [Ppie-1::mCherry::his-58; unc-119(+)] IV; ltIs38 [Ppie-1::gfp::PH(PLC1delta1); unc-119(+)]*